

Shear-horizontal transverse-electric seismoelectric waves in cylindrical double layer porous media

Wei-Hao Wang(王伟豪), Xiao-Yan Zhu(朱晓焱), Jin-Xia Liu(刘金霞), and Zhi-Wen Cui(崔志文)

Citation:CChin. Phys. B, 2021, 30 (**1**): 014301. DOI: 10.1088/1674-1056/abb308
Journal homepage: http://cpb.iphy.ac.cn; http://iopscience.iop.org/cpb

What follows is a list of articles you may be interested in

Symmetry-controlled edge states in graphene-like topological sonic crystal

Zhang-Zhao Yang(杨彰昭), Jin-Heng Chen(陈晋恒), Yao-Yin Peng(彭尧吟), Xin-Ye Zou(邹欣晔)
Chin. Phys. B, 2020, 29 (**10**): 104302. DOI: 10.1088/1674-1056/ab9c0e

Ultrasonic beam focusing characteristics of shear-vertical waves for contact-type linear phased array in solid

Yu-Xiang Dai(戴宇翔), Shou-Guo Yan(阎守国), Bi-Xing Zhang(张碧星)
Chin. Phys. B, 2020, 29 (**3**): 034304. DOI: 10.1088/1674-1056/ab69ed

Micro-crack detection of nonlinear Lamb wave propagation in three-dimensional plates with mixed-frequency excitation

Wei-Guang Zhu(祝伟光), Yi-Feng Li(李义丰), Li-Qiang Guan(关立强), Xi-Li Wan(万夕里), Hui-Yang Yu(余辉洋), Xiao-Zhou Liu(刘晓宙)
Chin. Phys. B, 2020, 29 (**1**): 014302. DOI: 10.1088/1674-1056/ab5931

Lamb waves topological imaging combining with Green's function retrieval theory to detect near filed defects in isotropic plates

Hui Zhang(张辉), Hai-Yan Zhang(张海燕), Meng-Yun Xu(徐梦云), Guo-Peng Fan(范国鹏), Wen-Fa Zhu(朱文发), Xiao-Dong Chai(柴晓冬)
Chin. Phys. B, 2019, 28 (**7**): 074301. DOI: 10.1088/1674-1056/28/7/074301

Manipulation of acoustic wavefront by transmissive metasurface based on pentamode metamaterials

Ying Liu(刘颖), Yi-Feng Li(李义丰), Xiao-Zhou Liu(刘晓宙)
Chin. Phys. B, 2019, 28 (**2**): 024301. DOI: 10.1088/1674-1056/28/2/024301

Shear-horizontal transverse-electric seismoelectric waves in cylindrical double layer porous media*

Wei-Hao Wang(王伟豪), Xiao-Yan Zhu(朱晓焱), Jin-Xia Liu(刘金霞), and Zhi-Wen Cui(崔志文)†

Department of Acoustics and Microwave Physics, College of Physics, Jilin University, Changchun 130012, *China*

(Received 20 June 2020; revised manuscript received 9 August 2020; accepted manuscript online 27 August 2020)

The shear-horizontal (SH) waves excited by the shear source in a borehole are easy to analyze due to the simple waveform. The borehole-side structures make the formation properties discontinuous. We consider a cylindrical double layer structure and study the borehole shear-horizontal and transverse-electric (SH-TE) seismoelectric waves. We first derive the expressions of the basic field quantities, and simulate the acoustic field and electric field using the real axis integral method. Compared with the wave fields of an infinitely homogeneous porous medium outside the borehole, the cylindrical layered structure makes the multi-mode cylindrical Love waves and their accompanying electric fields excited. Next, in order to study the interface response law of the inducing electric fields, we use the secant integral method to calculate the interface converted electromagnetic waves and analyze the causes of each component. It is found that an interface response occurs each time the SH wave impinges the interface in the layered porous medium. The results show that the SH-TE mode has a potential application for borehole-side interface detection in geophysical logs.

Keywords: seismoelectric effect, shear-horizontal and transverse-electric waves, cylindrical layer, porous media

PACS: 43.20.+g, 91.60.Lj, 91.30.f **DOI:** 10.1088/1674-1056/abb308

1. Introduction

The reservoirs of natural resources such as oil, water, and natural gases are mostly porous media. The seismoelectric effect related to the electric double layer in a fluid-containing porous medium has potential applications in many fields, e.g., resource exploration. Pride[1] derived the governing equations that control the coupled electromagnetic-seismic wave propagation. Since then, research on the seismoelectric effect has been widely carried out. Logging is one of the important means to obtain the formation information. Some scholars put forward the method of seismoelectric effect logging based on the experience of acoustic logging. This method receives both acoustic fields and electric fields, which can make up for the lack of information of a single type of wave field. In the seismoelectric logging method, the source and receivers are placed in the borehole, and not influenced by the detection depth.[2] Thus, the application prospect of the method in deep reservoir exploration is better. Hu *et al.*[3,4] carried out the earliest seismoelertric effect logging simulation. They discovered the electromagnetic head waves propagating at the formation electromagnetic wave velocity, which are independent of the acoustic field and reach the receivers almost simultaneously. In their follow-up work,[5] they proposed a simplified algorithm for calculating the inducing electric fields. Guan *et al.*[6] gave the rationality proof and applicable conditions for applying the simplified algorithm to calculate the borehole seismoelectric wave fields. Zyserman *et al.*[7] applied the method of surface seismoelectric logging exploration to study the problems of CO_2 storage and fluid seepage monitoring in the shallow surface. Guan *et al.*[8] used the finite-difference method to simulate the seismoelectric wave fields, the results are basically consistent with the simulation results obtained by real axis integral. When the formation outside the borehole is discontinuous, the characteristics of the seismoelectric coupling wave fields and the interface response law of the inducing electric fields are also important research directions. Ding *et al.*[9] simulated the borehole seismoelectric wave fields in a cylindrical layered formation with discontinuous salinity, the results show that an interface response will occur when the acoustic wave passes through the salinity difference interface. Zhao *et al.*[10] simulated the seismoelectric wave fields excited by a point acoustic source of a cylindrical double layer porous medium outside the borehole. Gao *et al.*[11] studied the propagation law of the acoustic-electric coupling waves in the porous elastic hollow cylinder in the fluid. Liu *et al.*[12] studied the seismoelectric coupling wave fields under the condition of logging while drilling with a cylindrical layered porous medium. The results show that the interface response will occur when the acoustic waves pass through the discontinuous formation. The more obvious the contrast of the elastic or electrical properties on interfaces in the layered porous medium, the stronger the interface response. The above studies are focused on the full-wave analysis of the seismoelectric coupling wave fields. The full wave waveform of the electric field becomes more complicated when the geolog-

*Project supported by the Natural Science Foundation of Jilin Province of China (Grant No. 20180101282JC) and the National Natural Science Foundation of China (Grant Nos. 40974067 and 42074139).

†Corresponding author. E-mail: cuizw@jlu.edu.cn

© 2021 Chinese Physical Society and IOP Publishing Ltd

ical structure outside the borehole is complicated. It is difficult to insight the interface response law of the electric field only from the full waveform. Component wave analysis of the seismoelectric wave fields is more helpful to reveal the relationship between the formation characteristics and the wave fields. Hu[13] used the method of secant integral to calculate the electromagnetic head wave. Wang *et al.*[14] conducted a comprehensive component wave analysis of the borehole seismoelectric wave fields excited by a point source. Wang *et al.*[15] studied the generation mechanism of the interface converted electromagnetic waves of a cylindrical layered porous formation. It was found that every time the formation fast p-wave and shear-horizontal-wave impinge the interface in the porous medium, an interface converted electromagnetic wave response will generate. In this paper, we also use the secant integral method to simulate the interface converted electromagnetic waves, and discuss the interface response law of shear-horizontal and transverse-electric (SH-TE) seismoelectric logging in a cylindrical double-layer porous medium.

The above research can well explain the characteristics of the borehole seismoelectric coupling wave fields excited by several typical acoustic sources. Due to the simple and easy analysis of the SH wave waveforms excited by the shear source, the work of shallow surface exploration using SH waves and the coupling electric fields has been widely carried out in recent years. Zyserman *et al.*[16] concluded that the signal-to-noise ratio of a shear wave source may be higher than that of a compressional source. Monachesi *et al.*[17] studied the seismoelectric response law of the SH waves excited by a surface shear source when passing through the seepage zone. In their subsequent work,[18] they studied the response law of the seismoelectric coupled waves excited by the horizontal shear source of the glacial environment. Gao *et al.*[19] used the finite difference method to simulate the 2D SH-TE seismoelectric waves. Munch *et al.*[20] investigated the possibility of using SH-TE seismoelectric coupling waves to detect non-aqueous fluid pollution in porous formations. In addition, related research has also shown that the borehole SH waves excited by the annular shear source have certain potential applications in formation exploration. White[21] first proposed the use of an annular shear source attached to the borehole wall for logging, and calculated the situation of a homogeneous medium outside the borehole. When it is a cylindrical layered medium outside the borehole, the characteristics of the acoustic field are different from the case of a homogeneous infinite medium. Yao *et al.*[22] studied the SH wave fields of a cylindrical double layer elastic medium outside the borehole. The results show that the wave field consists of the critically refracted SH wave and multi-order guided waves (i.e., cylindrical Love waves). Unlike the Love waves of the semi-infinite plate structure, the dispersion curve of each order Love wave has a cut-off frequency, which is caused by the bending of the interface. The Love wave phase velocity at the cut-off frequency is the SH wave velocity of the outer medium. When the frequency tends to infinity, the phase velocity of each order Love wave tends to the SH wave velocity of the inner medium. That is, the Love wave phase velocity range is $V_{s1} < V_{Love} < V_{s2}$, where V_{Love} is the phase velocity of the multi-mode Love waves, V_{s1} and V_{s2} are the SH wave velocities of the inner and the outer medium. In the cylindrical layered porous medium, the dispersion characteristics of Love waves are similar to those in an elastic medium, but the dispersion characteristics are affected by pore parameters.[23] Recent studies[24] have also shown that the circumferential guided waves in a porous cylinder are multi-order and dispersive. Relevant studies indicated that the seismoelectric effect logging method using the borehole SH-TE coupling waves also has certain potential applications in exploration. Cui *et al.*[25] simulated the borehole SH-TE coupling waves of an infinitely homogeneous saturated porous medium. When the formation outside the borehole is homogeneous, the acoustic field has only one component, namely the SH wave. The electric field has two components, which are the interface converted electromagnetic wave and the accompanying electric field of the SH wave. The interface converted electromagnetic waves propagate at the velocity of the formation electromagnetic waves, and the velocities of the accompanying electric fields and the SH waves are consistent. The presence of the borehole-side interface makes the elastic and electrical properties of the porous medium discontinuous. For this scenario, the formation can be regarded as a cylindrical layered porous medium. In order to analyze the borehole SH-TE coupling wave field characteristics of this situation and study the application potential in exploration, we construct an SH-TE acoustic-electric effect logging model for a cylindrical double layer porous medium in this study. The expressions of the basic field quantities inside and outside the borehole are derived, and the real axis integral method is used to simulate the time-domain waveforms. The wave field composition is also analyzed. Finally, in order to study the interface response law when the porous medium outside the borehole has an interface, we adopt the secant integral method to simulate the interface converted electromagnetic waves and analyze the causes of each component.

2. SH-TE seismoelectric waves

In this section, we first introduce the Pride governing equations and solve the complete coupling equations to obtain the expressions of the basic field quantities inside and outside the borehole. Then the real axis integral method is used to simulate the borehole SH-TE coupling wavefields of a cylindrical double layer porous medium and the wave field composition is also analyzed.

2.1. Expressions of the field quantities

Pride[1] combined Biot's[26] pore elastic wave equations and Maxwell's electromagnetic equations to derive the coupled acoustic-electromagnetic equations. The electrokinetic coupling effect is controlled by the following two equations:

$$\boldsymbol{J} = \sigma(\omega)\boldsymbol{E} + L(\omega)\left(-\nabla p + \omega^2 \rho_{\mathrm{f}} \boldsymbol{u}\right), \tag{1}$$

$$-\mathrm{i}\omega \boldsymbol{w} = L(\omega)\boldsymbol{E} + \left(-\nabla p + \omega^2 \rho_{\mathrm{f}} \boldsymbol{u}\right)\kappa(\omega)/\eta, \tag{2}$$

where $\boldsymbol{J}$ is the current density, $\boldsymbol{E}$ is the electric field strength; $\sigma(\omega)$, $\kappa(\omega)$ and $L(\omega)$ are the dynamic conductivity, the dynamic permeability and the electrokinetic coupling coefficient, respectively, which are all the functions of frequency; ρ_{f} is the pore fluid density, η is the viscosity coefficient of the pore fluid, $\boldsymbol{u}$ is the solid phase displacement; p is the pore fluid pressure, and $\boldsymbol{w}$ is the seepage displacement. Equation (1) shows that solid-phase displacement acceleration and pressure gradient can generate current, and the electric field can cause seepage. When the electrokinetic coupling coefficient $L(\omega)$ is zero, the acoustic field is decoupled from the electric field, and the Pride governing equations will degenerate into Biot's pore elastic wave equations and Maxwell's electromagnetic equations.

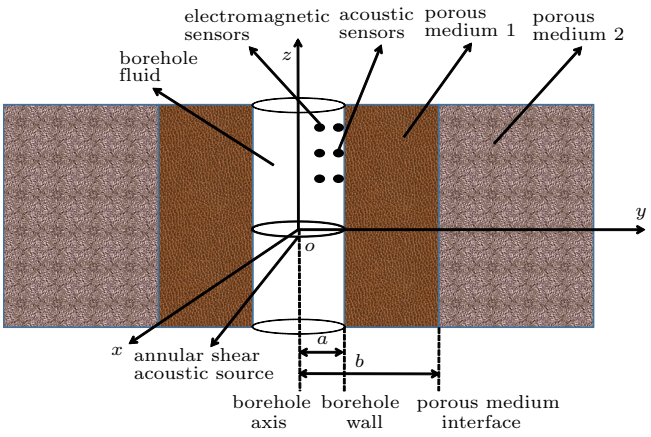


Fig. 1. Schematic diagram of SH-TE seismioelectric effect logging.

Solving the above complete Pride governing equations, the frequency-wavenumber domain expressions of the basic field quantities can be obtained. We study the SH-TE seismoelectric effect logging problem of a cylindrical double-layered porous medium. The model schematic diagram is shown in Fig. 1. The radius of the borehole is $a = 0.1$ m, and the distance between the interface of the porous medium and the borehole axis is $b = 1.5$ m. There is an annular shear acoustic source attached to the borehole. The acoustic receivers are placed on the borehole wall and the electromagnetic receivers are placed in the borehole fluid. The radial distance of the electromagnetic receivers from the borehole axis is half the borehole radius. Porous medium 1 is a finite thickness porous medium, and porous medium 2 is infinite.

Since the acoustic source is an annular shear source, the axial electric field cannot be excited. According to Cui *et al.*,[25] the frequency-wavenumber domain expressions of the basic field quantities of the borehole fluid and the outermost infinite porous medium are given by

$$\hat{E}_\theta^{\mathrm{b}} = \frac{\mathrm{i}}{\eta_{\mathrm{e}}}\omega\mu A_H I_1(\eta_{\mathrm{e}} r), \tag{3}$$

$$\hat{H}_r^{\mathrm{b}} = -\frac{\mathrm{i}}{\eta_{\mathrm{e}}} k_z A_H I_1(\eta_{\mathrm{e}} r), \tag{4}$$

$$\hat{u_\theta^{\mathrm{o}}} = \eta_{\mathrm{sh}}^{\mathrm{o}} K_1(\eta_{\mathrm{sh}}^{\mathrm{o}} r) B_{\mathrm{sh}}^{\mathrm{o}} + \eta_{\mathrm{em}}^{\mathrm{o}} K_1(\eta_{\mathrm{em}}^{\mathrm{o}} r) B_{\mathrm{em}}^{\mathrm{o}}, \tag{5}$$

$$\hat{\tau_{r\theta}^{\mathrm{o}}} = -G^{\mathrm{o}}\left[\eta_{\mathrm{sh}}^{\mathrm{o}\,2} K_2(\eta_{\mathrm{sh}}^{\mathrm{o}} r) B_{\mathrm{sh}}^{\mathrm{o}} + \eta_{\mathrm{em}}^{\mathrm{o}\,2} K_2(\eta_{\mathrm{em}}^{\mathrm{o}} r) B_{\mathrm{em}}^{\mathrm{o}}\right], \tag{6}$$

$$\hat{E_\theta^{\mathrm{o}}} = \beta_{\mathrm{sh}}^{\mathrm{o}} \eta_{\mathrm{sh}}^{\mathrm{o}} K_1(\eta_{\mathrm{sh}}^{\mathrm{o}} r) B_{\mathrm{sh}}^{\mathrm{o}} + \beta_{\mathrm{em}}^{\mathrm{o}} \eta_{\mathrm{em}}^{\mathrm{o}} K_1(\eta_{\mathrm{em}}^{\mathrm{o}} r) B_{\mathrm{em}}^{\mathrm{o}}, \tag{7}$$

$$\hat{H_z^{\mathrm{o}}} = \frac{\mathrm{i}}{\omega\mu}\left[\beta_{\mathrm{sh}}^{\mathrm{o}} \eta_{\mathrm{sh}}^{\mathrm{o}\,2} K_0(\eta_{\mathrm{sh}}^{\mathrm{o}} r) B_{\mathrm{sh}}^{\mathrm{o}} + \beta_{\mathrm{em}}^{\mathrm{o}} \eta_{\mathrm{em}}^{\mathrm{o}\,2} K_0(\eta_{\mathrm{em}}^{\mathrm{o}} r) B_{\mathrm{em}}^{\mathrm{o}}\right], \tag{8}$$

where $\hat{E}_\theta^{\mathrm{b}}$ and $\hat{H}_r^{\mathrm{b}}$ are the tangential electric field and the radial magnetic field of the borehole fluid; $\hat{u_\theta^{\mathrm{o}}}$, $\hat{\tau_{r\theta}^{\mathrm{o}}}$, $\hat{E_\theta^{\mathrm{o}}}$ and $\hat{H_z^{\mathrm{o}}}$ are the tangential displacement, tangential stress, tangential electric field and axial magnetic field of the outermost infinite formation, respectively; μ is the magnetic permeability and G^{o} is the shear modulus of the outermost porous medium; η_{e} is the electromagnetic radial wave number of the borehole fluid; $\eta_{\mathrm{sh}}^{\mathrm{o}}$ and $\eta_{\mathrm{em}}^{\mathrm{o}}$ are the radial wave numbers of the SH wave and the electromagnetic wave of the outermost infinite porous medium, respectively; k_z is the axial wave number. A_H is the undetermined coefficient related to the electromagnetic fields of the borehole, also known as the response coefficient of the borehole electromagnetic fields. $B_{\mathrm{sh}}^{\mathrm{o}}$ and $B_{\mathrm{em}}^{\mathrm{o}}$ are also the undetermined coefficients; $\beta_{\mathrm{sh}}^{\mathrm{o}}$ is the ratio of the shear wave component of the electric field to the shear wave component of the solid phase displacement; $1/\beta_{\mathrm{em}}^{\mathrm{o}}$ is the ratio of the electromagnetic wave component of the solid phase displacement to the electromagnetic wave component of the electric field;[1] r is the radial distance between the field point and the borehole axis. K_0, I_1, K_1, and K_2 are the imaginary variation Bessel functions. In a similar way, we can obtain the frequency-wavenumber domain expressions of the basic field quantities of the inner porous medium as follows:

$$\begin{aligned}\hat{u_\theta} = {} & \eta_{\mathrm{sh}} K_1(\eta_{\mathrm{sh}} r) B_{\mathrm{sh}} - \eta_{\mathrm{sh}} I_1(\eta_{\mathrm{sh}} r) A_{\mathrm{sh}} \\ & + \eta_{\mathrm{em}} K_1(\eta_{\mathrm{em}} r) B_{\mathrm{em}} - \eta_{\mathrm{em}} I_1(\eta_{\mathrm{em}} r) A_{\mathrm{em}},\end{aligned} \tag{9}$$

$$\begin{aligned}\hat{E_\theta} = {} & \beta_{\mathrm{sh}}\eta_{\mathrm{sh}} K_1(\eta_{\mathrm{sh}} r) B_{\mathrm{sh}} - \beta_{\mathrm{sh}}\eta_{\mathrm{sh}} I_1(\eta_{\mathrm{sh}} r) A_{\mathrm{sh}} \\ & + \beta_{\mathrm{em}}\eta_{\mathrm{em}} K_1(\eta_{\mathrm{em}} r) B_{\mathrm{em}} - \beta_{\mathrm{em}}\eta_{\mathrm{em}} I_1(\eta_{\mathrm{em}} r) A_{\mathrm{em}},\end{aligned} \tag{10}$$

$$\begin{aligned}\hat{\tau_{r\theta}} = {} & -G^{\mathrm{i}}[\eta_{\mathrm{sh}}^2 K_2(\eta_{\mathrm{sh}} r) B_{\mathrm{sh}} + \eta_{\mathrm{sh}}^2 I_2(\eta_{\mathrm{sh}} r) A_{\mathrm{sh}} \\ & + \eta_{\mathrm{em}}^2 K_2(\eta_{\mathrm{em}} r) B_{\mathrm{em}} + \eta_{\mathrm{em}}^2 I_2(\eta_{\mathrm{em}} r) A_{\mathrm{em}}],\end{aligned} \tag{11}$$

$$\begin{aligned}\hat{H}_z = {} & \frac{\mathrm{i}}{\omega\mu}[\beta_{\mathrm{sh}}\eta_{\mathrm{sh}}^2 K_0(\eta_{\mathrm{sh}} r) B_{\mathrm{sh}} + \beta_{\mathrm{sh}}\eta_{\mathrm{sh}}^2 I_0(\eta_{\mathrm{sh}} r) A_{\mathrm{sh}} \\ & + \beta_{\mathrm{em}}\eta_{\mathrm{em}}^2 K_0(\eta_{\mathrm{em}} r) B_{\mathrm{e}} + \beta_{\mathrm{em}}\eta_{\mathrm{em}}^2 I_0(\eta_{\mathrm{em}} r) A_{\mathrm{sh}}].\end{aligned} \tag{12}$$

In Eqs. (9)–(12), $\hat{u_\theta}$, $\hat{E_\theta}$, $\hat{\tau_{r\theta}}$ and $\hat{H_z}$ are the tangential displacement, tangential electric field, tangential stress and axial magnetic field of the inner porous medium, respectively; $\eta_{\rm sh}^2 = k_z^2 - k_{\rm sh}^2$ and $\eta_{\rm em}^2 = k_z^2 - k_{\rm em}^2$ are the radial wave numbers of the SH wave and the electromagnetic wave of the inner porous medium, respectively. Here $k_{\rm sh}$ and $k_{\rm sh}$ are the SH wave and electromagnetic wave numbers of the inner porous medium, respectively. $A_{\rm sh}$, $B_{\rm sh}$, $A_{\rm em}$ and $B_{\rm em}$ are the undetermined coefficients. $G^{\rm i}$ is the shear modulus of the inner porous medium. I_0 and I_2 are the imaginary variation Bessel functions. The boundary conditions at the borehole wall and the interface of the porous medium are given in the following.

At the borehole wall ($r = a$):

$$\tau_{r\theta}^{\rm o} = \tau_{\rm s}^{\rm b}, \quad E_\theta^{\rm o} = E_\theta^{\rm b}, \quad H_z^{\rm o} = H_z^{\rm b}. \tag{13}$$

At the interface of porous medium ($r = b$):

$$u_\theta = u_\theta^{\rm o}, \quad \tau_{r\theta} = \tau_{r\theta}^{\rm o}, \quad E_\theta = E_\theta^{\rm o}, \quad H_z = H_z^{\rm o}. \tag{14}$$

Substituting the field expressions of the interlayer porous medium, the borehole fluid and the outermost porous medium into the boundary conditions (13) and (14), we can reach the matrix equations

$$[m_{ij}]_{7\times7} \cdot [A_j]_{7\times1} = [B_j]_{7\times1}, \tag{15}$$

$$[A_j]_{7\times1} = [A_H,\ B_{\rm sh},\ B_{\rm em},\ A_{\rm sh},\ A_{\rm em},\ B_{\rm sh}^{\rm o},\ A_{\rm em}^{\rm o}]^{\rm T}, \tag{16}$$

$$[B_j]_{7\times1} = \left[\tau_{\rm s}^{\rm b},\ 0,\ 0,\ 0,\ 0,\ 0,\ 0\right]^{\rm T}. \tag{17}$$

Here $[m_{ij}]_{7\times7}$ is the coefficient matrix and the matrix elements are given in the Appendix. $[A_j]_{7\times1}$ is the matrix of the undetermined coefficients. $[B_j]_{7\times1}$ is determined by the source, $\tau_{\rm s}^{\rm b}$ is a tangential stress source. We take $\tau_{\rm s}^{\rm b} = G^{\rm i} \times 10^{-3}$. Solving the equations and determining the undetermined coefficients, then substituting the coefficients into the field quantity expressions, we can finally obtain the wave fields in each region.

2.2. Numerical simulation results

In this part, the real axis integral method is used to simulate the coupled acoustic and electromagnetic wave fields. The parameters of the layered porous medium are given in Table 1, they are the typical sandstone parameters.[4,16] In addition, the fluid density in the borehole is 1000 kg/m^3, and the salinity is 0.01 Mol/L. The central frequency of the acoustic source is 10 kHz.

Under low frequency approximation, the SH wave velocity of the porous medium is given by $V_{\rm s} = \sqrt{G/\rho}$, $V_{\rm s}$ is the velocity of the SH wave and ρ is the density of the porous medium, $\rho = \phi\rho_{\rm f} + (1-\phi)\rho_{\rm s}$. Combined the parameters given in Table 1, we can calculate the inner and outer porous medium SH wave velocities to be $V_{\rm s1} = 1378.7$ m/s and $V_{\rm s2} = 2474.7$ m/s, respectively. Figure 2 shows the normalized amplitudes of the SH-TE coupled acoustic and electromagnetic fields of different source distances. The solid lines are the electric field full waves E_θ, the dashed lines are the acoustic field full waves u_θ, and z is the source distance.

Table 1. Porous medium parameters.

Parameters	Symbols	Units	Porous medium 1	Porous medium 2
Porosity	ϕ	1	0.20	0.18
Permeability	κ	μm^2	0.01	0.01
Frame Shear modulus	G	GPa	4.10	14.40
Frame density	$\rho_{\rm s}$	kg/m^3	2650	2650
Pore fluid density	$\rho_{\rm f}$	kg/m^3	1000	1000
Frame permittivity	$\varepsilon_{\rm s}$	ε_0	3	3
Fluid permittivity	$\varepsilon_{\rm f}$	ε_0	80	80
Salinity	C	Mol/L	0.01	0.001
Fluid viscosity	$\eta_{\rm w}$	Pa·s	0.001	0.001
Tortuosity	α_∞	1	2.0	1.9

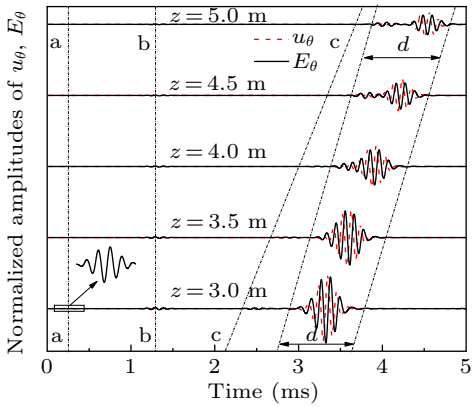


Fig. 2. Borehole SH-TE seismoelectric wave fields of a cylindrical double layer porous medium. The solid and dashed lines correspond to the electric and acoustic fields, respectively.

Compared with the homogeneous medium,[25] when the porous medium outside the borehole is a cylindrical double layer porous medium, the components of the acoustic field and the electric field become complicated. Due to $V_{\rm s1} < V_{\rm s2}$, the cylindrical Love waves can be excited.[22,23] The acoustic field is composed of two parts, which are represented as c–c, d–d in Fig. 2, respectively. The component c–c is the critically refracted SH wave, it propagates at the SH wave velocity of the outer porous medium. The component d–d is composed of multi-order Love waves. The electric field consists of four components. When the source distance increases, the arrival time of components a–a and b–b is almost unchanged. This shows that components a–a and b–b are the interface responses, they are generated by the SH waves impinging the interface of the medium and propagate at the velocity of the formation electromagnetic waves, also called the interface converted electromagnetic waves. This is consistent with the interface response characteristics of the borehole seismoelectric coupling wave fields excited by a point acoustic source.[3–5] After the interface responses a–a and b–b, the electric field component c–c is the accompanying electric field of the SH wave. The electric field component d–d is the accompanying electric field of the multi-mode Love waves. Since the propagating velocity of the accompanying electric fields of the Love waves are the same as the Love wave velocities,[3,4,25] the dis-

persion law for them is also the same. The dispersion characteristics of the Love waves in a cylindrical layered porous medium can refer to Ref. [23]. In a nutshell, as the frequency increases, the phase velocity of the Love wave gradually decreases, and the phase velocity of each order Love wave is greater than the SH wave velocity of the inner layer porous medium and less than the SH wave velocity of the outer layer porous medium.

3. Interface response

In order to study the interface response of the borehole SH-TE seismoelectric coupling wave fields when the porous medium has an interface, we use the secant integral method to calculate the interface converted electromagnetic waves. The interface converted electromagnetic waves refer to the electromagnetic wave components generated by the SH wave impinging the interface of the medium and propagate at the velocity of the formation electromagnetic wave.[13,25] In this section, we first introduce the basic theory of the vertical secant integral and simulate the time domain waveforms of the interface converted electromagnetic waves. Next, the cause of each component is analyzed by comparing the interface converted electromagnetic wave waveforms of different interface positions.

3.1. The secant integral theory

In the complex plane, what correspond to the critical refraction waves (also called the interface waves) is the contribution of the secant integral of the body wave branch points. Pride *et al.*[27] proposed that there are totally four kinds of body waves in the porous medium, which are the fast p-wave, the SH wave, the slow p-wave and the electromagnetic wave (EM wave). Since the acoustic source is an annular shear source attached to the borehole wall, there are only two kinds of body waves in the formation, which are the SH wave and the EM wave. The branch point values of the formation body wave are given by $k_j = \sqrt{\omega/c_j}$, where k_j represents some kind of body wave branch point in the formation, c_j represents the wave velocity of the corresponding body wave. Combining the above expression and the media parameters in Table 1, we give the values of the branch points of the formation body wave in Table 2. Here $k_{\rm sh}^{\rm o}$ and $k_{\rm em}^{\rm o}$ are the SH wave and the electromagnetic wave branch points corresponding to the outermost infinite porous medium, respectively; $k_{\rm sh}$ and $k_{\rm em}$ are the SH wave and the electromagnetic wave branch points corresponding to the inner porous medium, respectively. According to Table 2, Fig. 3 shows the distribution of the formation body wave branch points and the integral path in the k_z complex plane, the arrows in Fig. 3 indicate the integral path.

According to the related work,[14,28,29] in the cylindrical multilayer medium, the branch points corresponding to the borehole fluid and the inner medium are non-substantial branch points. Only the body wave branch points corresponding to the outermost infinite medium are substantial. Therefore, $k_{\rm sh}$ and $k_{\rm em}$ in Fig. 3 are both non-substantial branch points. The simulation results of the interface converted electromagnetic waves are obtained by calculating the secant integral of the electromagnetic wave branch point $k_{\rm em}^{\rm o}$. The value of the electromagnetic wave branch point secant integral is given by

$$I_{E_{\theta\rm cut}}(\omega,z) = \frac{\mathrm{i}\omega\mu}{\eta_{\rm e}} \int_{\rm cut} \left[A_{\rm H}^{+}(k,\omega) - A_{\rm H}^{-}(k,\omega)\right] \mathrm{e}^{\mathrm{i}k_z z}\mathrm{d}k_z, \quad (18)$$

where $I_{E_{\theta\rm cut}}(\omega,z)$ represents the secant integral value of $k_{\rm em}^{\rm o}$. $A_{\rm H}^{+}(k,\omega)$ and $A_{\rm H}^{-}(k,\omega)$ are the values of the electromagnetic response coefficient on the right bank and the left bank of the vertical secant respectively; "cut" represents the integral path from the electromagnetic wave branch point to positive infinity. By solving Eq. (18), we can obtain the secant integral value of the electromagnetic wave branch point, and then the interface converted electromagnetic wave can be obtained.

Table 2. Values of the formation body wave branch points.

Branch points	$k_{\rm em}^{\rm o}$	$k_{\rm em}$	$k_{\rm sh}^{\rm o}$	$k_{\rm sh}$
Values/m^{-1}	4.76×10^{-3}	1.49×10^{-2}	15.3	28.4

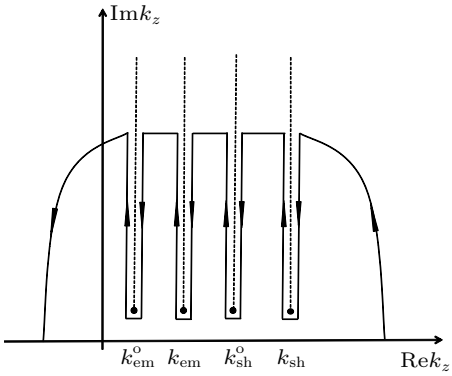


Fig. 3. Distribution of the body wave branch points and the integral path.

3.2. Interface converted electromagnetic wave

Figure 4 shows the normalized time domain waveforms of the interface converted electromagnetic wave when the formation outside the borehole is a cylindrical double layer porous medium. The parameters adopted in this section are the same as those in Table 1. The distance between the interface of the porous medium and the borehole axis is still 1.5 m, and the axial distance of the electromagnetic sensors from the borehole axis is half the radius of the borehole. In order to distinguish it from the tangential electric field full wave E_θ obtained in the previous section, we represent the interface converted electromagnetic waves calculated by secant integral as $E_{\theta\rm cut}$.

The interface converted electromagnetic wave is composed of three components, which are represented as a–a, b–b,

and c–c in Fig. 4. The arrival time of each component of the interface converted electromagnetic wave hardly increases with the increasing source distance. In order to illustrate the component corresponding relationship between the interface converted electromagnetic wave $E_{\theta\text{cut}}$ and the electric field full wave E_θ, Fig. 5 shows the waveform comparison of $E_{\theta\text{cut}}$ and E_θ. Here we take the waveforms with a source distance of 3 m as an example. The upper figure is the waveform of the electric field full wave and the lower one is the waveform of the interface converted electromagnetic. They are both normalized with their respective maximum amplitudes.

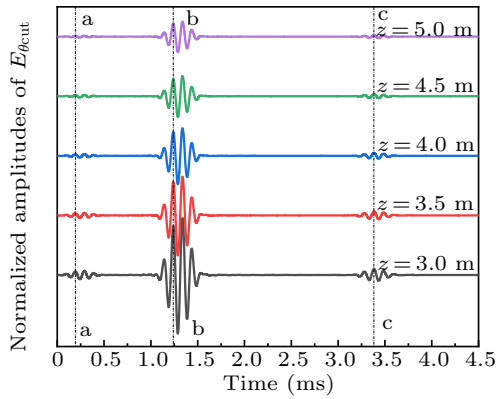


Fig. 4. Normalized amplitudes of the interface converted electromagnetic wave.

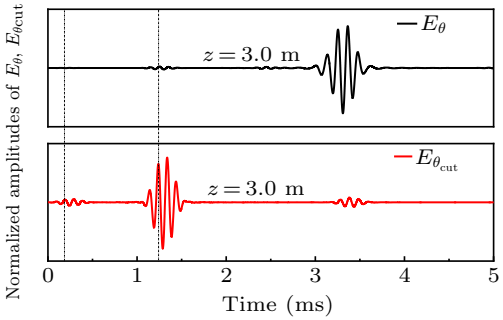


Fig. 5. Waveform comparison of the interface converted electric wave and the electric field full wave.

From comparison, we can find that the first two components of the interface electromagnetic wave $E_{\theta\text{cut}}$ and the electric field full wave E_θ are correspondence. This further illustrates that the components a–a and b–b in the full wave of the electric field given by Fig. 2 are the interface converted electromagnetic waves. Since the amplitude of the interface converted electromagnetic wave component c–c in Fig. 4 is small and the arrival time is close to the accompanying electric fields, it is not obvious in the electric field full wave E_θ. In order to explain the production causes of each component of $E_{\theta\text{cut}}$, we compare the waveforms of $E_{\theta\text{cut}}$ of different porous medium interface positions, as shown in Fig. 6. Δt_1 and Δt_2 are the arrival time difference, b is the distance between the porous medium interface and the borehole axis. Here we still take the waveforms with a source distance of 3 m as an example.

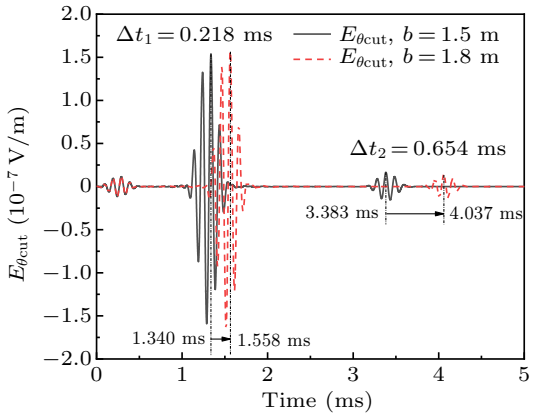


Fig. 6. Interface converted electromagnetic waveforms of different interface positions. The solid and the dashed line correspond to $b = 1.5$ m and 1.8 m, respectively.

As shown in Fig. 6, when the porous medium interface turns 0.3 m away from the borehole wall, the arrival time and the amplitude of the first component hardly change. The position of the interface has little influence on the first component. This shows that the first component (represented as a–a in Fig. 4) is the interface response at the borehole wall. The arrival time difference of the second component is 0.218 ms, which is consistent with the time of SH wave propagating 0.3 m in the inner porous medium. This shows that the second component (represented as b–b Fig. 4) is the interface response generated by the SH wave impinging the interface of the porous medium. The arrival time difference of the third component is 0.654 ms, which is consistent with the time of SH wave propagating 0.9 m in the inner medium. This shows that the third component (represented as c–c in Fig. 4) is the interface response generated by the SH wave impinging the interface of the porous medium again after two reflections. Since the SH wave is uncoupled with the fluid in the borehole, there is almost no interface response when the SH wave propagates back from the formation to the borehole wall. In summary, the first component of the interface converted electromagnetic wave is the interface response at the borehole wall. Except for the first component, all the other components are the interface responses generated by the SH wave impinging the interface between the porous medium.

4. Conclusions

In summary, we have studied the borehole SH-TE seismoelectric coupling wave fields of a cylindrical double layer porous medium. First, we derive the expressions of the basic field quantities inside and outside the borehole, and the full wave waveforms of the acoustic field and electric field are simulated. Then, in order to study the interface response, we use the secant integral method to calculate the interface converted electromagnetic waves. The results show that the interface of the porous medium makes the composition of the acoustic-electric coupling wave fields more complicated than that of a

homogeneous infinite medium. In addition to the critically refracted SH waves, multi-order and dispersive cylindrical Love waves can also be excited due to the layered structure. The electric field includes the interface responses and the accompanying electric fields of the acoustic fields. The interface converted electromagnetic waves propagate in the porous medium at the velocity of the formation electromagnetic waves while the accompanying electric fields are consistent with the propagation velocity of the acoustic waves. The existence of the interface of the porous medium makes the interface response law of the SH-TE wave fields complicated. The results show that when the SH wave generate multi refractions and reflections in the inner porous medium, each time it impinges the interface between the porous medium, an interface converted electromagnetic wave response will occur. The research results in this study indicate that the borehole SH-TE seismoelectric coupling wave fields have certain application potential in the fields of formation exploration and borehole-side interface detection. However, the Love waves in the porous layered medium are complicated. The dispersion, excitation and attenuation characteristics of the cylindrical Love modes with seismoelectric effect are worthy of further study. In addition, the idealized model in this paper needs further improvement to be more in line with the actual situation.

5. Appendix A

The elements of matrix $[m_{ij}]_{7\times7}$ are

$$
\begin{aligned}
&m_{11}=0; && m_{21}=\tfrac{\mathrm{i}\omega\mu}{\eta_{\mathrm{e}}}I_1(\eta_{\mathrm{e}}a);\\
&m_{12}=-G^{\mathrm{i}}\eta_{\mathrm{sh}}^2K_2(\eta_{\mathrm{sh}}a); && m_{22}=-\beta_{\mathrm{sh}}\eta_{\mathrm{sh}}K_1(\eta_{\mathrm{sh}}a);\\
&m_{13}=-G^{\mathrm{i}}\eta_{\mathrm{em}}^2K_2(\eta_{\mathrm{em}}a); && m_{23}=-\beta_{\mathrm{em}}\eta_{\mathrm{em}}K_1(\eta_{\mathrm{em}}a);\\
&m_{14}=-G^{\mathrm{i}}\eta_{\mathrm{sh}}^2I_2(\eta_{\mathrm{sh}}a); && m_{24}=\beta_{\mathrm{sh}}\eta_{\mathrm{sh}}I_1(\eta_{\mathrm{sh}}a);\\
&m_{15}=-G^{\mathrm{i}}\eta_{\mathrm{em}}^2I_2(\eta_{\mathrm{em}}a); && m_{25}=\beta_{\mathrm{em}}\eta_{\mathrm{em}}I_1(\eta_{\mathrm{em}}a);\\
&m_{16}=0;\ \ m_{17}=0; && m_{26}=0;\ \ m_{27}=0;\\
&m_{31}=I_0(\eta_{\mathrm{e}}a); && m_{41}=0;\\
&m_{32}=-\tfrac{\mathrm{i}}{\omega\mu}\eta_{\mathrm{sh}}^2\beta_{\mathrm{sh}}K_0(\eta_{\mathrm{sh}}a); && m_{42}=-G^{\mathrm{i}}\eta_{\mathrm{sh}}^2K_2(\eta_{\mathrm{sh}}b);\\
&m_{33}=-\tfrac{\mathrm{i}}{\omega\mu}\eta_{\mathrm{em}}^2\beta_{\mathrm{em}}K_0(\eta_{\mathrm{em}}a); && m_{43}=-G^{\mathrm{i}}\eta_{\mathrm{em}}^2K_2(\eta_{\mathrm{em}}b);\\
&m_{34}=-\tfrac{\mathrm{i}}{\omega\mu}\eta_{\mathrm{sh}}^2\beta_{\mathrm{sh}}I_0(\eta_{\mathrm{sh}}a); && m_{44}=-G^{\mathrm{i}}\eta_{\mathrm{sh}}^2I_2(\eta_{\mathrm{sh}}b);\\
&m_{35}=-\tfrac{\mathrm{i}}{\omega\mu}\eta_{\mathrm{em}}^2\beta_{\mathrm{em}}I_0(\eta_{\mathrm{em}}a); && m_{45}=-G^{\mathrm{i}}\eta_{\mathrm{em}}^2I_2(\eta_{\mathrm{em}}b);\\
&m_{36}=0;\ \ m_{37}=0; && m_{46}=G^{\mathrm{o}}{\eta_{\mathrm{sh}}^{\mathrm{o}}}^2K_2(\eta_{\mathrm{sh}}^{\mathrm{o}}b);\\
&m_{51}=0;\ \ m_{61}=0; && m_{47}=G^{\mathrm{o}}{\eta_{\mathrm{em}}^{\mathrm{o}}}^2K_2(\eta_{\mathrm{em}}^{\mathrm{o}}b);\\
&m_{52}=\eta_{\mathrm{sh}}K_1(\eta_{\mathrm{sh}}b); && m_{62}=\beta_{\mathrm{sh}}\eta_{\mathrm{sh}}K_1(\eta_{\mathrm{sh}}b);\\
&m_{53}=\eta_{\mathrm{em}}K_1(\eta_{\mathrm{em}}b); && m_{63}=\beta_{\mathrm{em}}\eta_{\mathrm{em}}K_1(\eta_{\mathrm{em}}b);\\
&m_{54}=-\eta_{\mathrm{sh}}I_1(\eta_{\mathrm{sh}}b); && m_{64}=-\beta_{\mathrm{sh}}\eta_{\mathrm{sh}}I_1(\eta_{\mathrm{sh}}b);\\
&m_{55}=-\eta_{\mathrm{em}}I_1(\eta_{\mathrm{em}}b); && m_{65}=-\beta_{\mathrm{em}}\eta_{\mathrm{em}}I_1(\eta_{\mathrm{em}}b);\\
&m_{56}=\eta_{\mathrm{sh}}^{\mathrm{o}}K_1(\eta_{\mathrm{sh}}^{\mathrm{o}}b); && m_{66}=-\beta_{\mathrm{sh}}^{\mathrm{o}}\eta_{\mathrm{sh}}^{\mathrm{o}}K_1(\eta_{\mathrm{sh}}^{\mathrm{o}}b);\\
&m_{57}=\eta_{\mathrm{em}}^{\mathrm{o}}K_1(\eta_{\mathrm{em}}^{\mathrm{o}}b); && m_{67}=-\beta_{\mathrm{em}}^{\mathrm{o}}\eta_{\mathrm{em}}^{\mathrm{o}}K_1(\eta_{\mathrm{em}}^{\mathrm{o}}b);\\
&m_{71}=0; && m_{72}=\eta_{\mathrm{sh}}^2\beta_{\mathrm{sh}}K_0(\eta_{\mathrm{sh}}b);\\
&m_{73}=\eta_{\mathrm{em}}^2\beta_{\mathrm{em}}K_0(\eta_{\mathrm{em}}b); && m_{74}=\eta_{\mathrm{sh}}^2\beta_{\mathrm{sh}}I_0(\eta_{\mathrm{sh}}b);\\
&m_{75}=\eta_{\mathrm{em}}^2\beta_{\mathrm{em}}I_0(\eta_{\mathrm{em}}b); && m_{76}=-{\eta_{\mathrm{sh}}^{\mathrm{o}}}^2\beta_{\mathrm{sh}}^{\mathrm{o}}K_0(\eta_{\mathrm{sh}}^{\mathrm{o}}b);\\
&m_{77}=-{\eta_{\mathrm{em}}^{\mathrm{o}}}^2\beta_{\mathrm{em}}^{\mathrm{o}}K_0(\eta_{\mathrm{em}}^{\mathrm{o}}b).
\end{aligned}
$$

Here a is the borehole radius, and b is the distance between the interface of the porous medium and the borehole axis.

References

[1] Pride S R 1994 *Phys. Rev. B* **50** 15678
[2] Zhu Z, Haartsen M W and Toksöz M N 1999 *Geophysics* **64** 1349
[3] Hu H and Wang K X 1999 *Well Logging Technology* **23** 427 (in Chinese)
[4] Hu H and Wang K X 2000 *Well Logging Technology* **24** 3 (in Chinese)
[5] Hu H S and Liu J 2002 *Proceedings of the 72nd SEG Annual International Meeting*, 6–11 October 2002, Salt Lake City, Utah, USA, p. 348
[6] Guan W, Shi P and Hu H S 2018 *Geophys. J. Int.* **212** 458
[7] Zyserman F, Jouniaux L, Warden S and Garambois S 2015 *Int. J. Greenhouse Gas Control* **33** 89
[8] Guan W and Hu H S 2008 *J. Comput. Phys.* **227** 5633
[9] Ding H R, Liu J X, Cui Z W and Tribikram Kundu 2017 *Chin. Phys. B* **26** 124301
[10] Zhao Y J, Ding H R, Cui Z W and Wang K X 2016 *Tech. Acoust.* **35** 258 (in Chinese)
[11] Gao W Y, Cui Z W and Wang K X 2013 *J. Sound. Vib.* **332** 5014
[12] Liu Y K, Tang X M and Su Y D 2016 *Chin. J. Geophys.* **59** 1898
[13] Hu H S 2003 *Acta Phys. Sin.* **52** 1954 (in Chinese)
[14] Wang Z, Hu H S, Guan W and He X 2012 *Acta Phys. Sin.* **61** 054302 (in Chinese)
[15] Wang W H and Cui Z W 2019 *Acta Phys. Sin.* **68** 152 (in Chinese)
[16] Zyserman F, Monachesi L and Jouniaux L 2017 *Geophys. J. Int.* **208** 918
[17] Monachesi L, Zyserman F and Jouniaux L 2018 *Geophys. J. Int.* **213** 1999
[18] Monachesi L, Zyserman F and Jouniaux J 2018 *J. Geophys. Res.: Earth Surf.* **123** 2135
[19] Gao Y X, Wang D D, Yao C, Guan W, Hu H S, Wen J, Zhang W, Tong P and Yang Q J 2019 *Geophys. J. Int.* **216** 414
[20] Munch F D and Zyserman F I 2016 *J. Appl. Geophys.* **130** 8
[21] White J E 1991 *The Log. Analyst.* **3** 242
[22] Yao G J, Wang K X, Ma J and White J E 2005 *J. Geophys. Engin.* **2** 169
[23] Yao G J 2000 *Impedance inversion and application of ultrasonic reflection method in casing well and analysis of cylindrical Love waves and theoretical study of excitation of SH wave field* (Ph.D. Dissertation) (Changchun: Jilin University) (in Chinese)
[24] Su N N, Han Q B and Jiang J 2019 *Acta Phys. Sin.* **68** 150 (in Chinese)
[25] Cui Z, Wang K X, Sun J G, Zhu Z, Yao G and Hu H S 2007 *Chin. Phys. Lett.* **24** 3454
[26] Biot M A 1962 *J. Appl. Phys.* **33** 1482
[27] Pride S R and Harrtsen M W 1996 *J. Acoust. Soc. Am.* **100** 1301
[28] Chew W C 1983 *IEEE Trans. Anten. Propagat.* **31** 653
[29] Kurkjian A L 1985 *Geophysics* **50** 852